



Effects of Spray Parameters on the YSZ-Alumina Splat Formation During Solution Precursor High Velocity Flame Spraying

Saeid Taghi-Ramezani¹ · Zia Valefi¹

Received: 15 April 2023 / Accepted: 24 September 2023 / Published online: 16 October 2023
© The Author(s) under exclusive licence to The Korean Institute of Metals and Materials 2023

Abstract

Solution precursor thermal spraying (SPTS) processes that have been successfully developed, are suitable methods for producing nanostructured coatings. In the SPTS coatings, important features are splat, porosity, un-melted particles and un-pyrolysed precursor. Such features can be studied by observing deposit collected by spraying only a single pass on to the substrate. In the present study, deposition of YSZ-40 wt% Al₂O₃ on glass substrates by solution precursor high velocity flame spraying (SP-HVFS) of zirconium oxy nitrate, yttrium nitrate and aluminum nitrate solutions mixed with suitable percentage to result YSZ-40 wt% Al₂O₃ in single scan experiment has been studied/for the first time. In order to investigate the SP-HVFS process, all spraying parameters including the fuel-oxygen ratio, the spraying distance and the feed rate of solution precursor were varied. The results of thermal analysis showed that precursor decomposition is an exothermic reaction that mainly occurs at temperatures above 250 °C. Also, the phase compositions of the YSZ-40 wt% Al₂O₃ powders resulted from pyrolysis of the precursor in furnace at different temperatures were investigated by X-ray diffraction, which confirmed that with increasing heat treatment temperature, the degree of crystallinity and grain size of YSZ-40 wt% Al₂O₃ powder increases. The morphology of the deposits formed on the glass substrates and their structural characteristics were studied using Field Emission Scanning Electron Microscope. Structural comparison of deposits formed on glass substrates in the single scan experiment showed that at low fuel and oxygen flow rates (30 and 300 l/min respectively), solution precursor injection rate of 20 cm³/min and spray distance of 5 cm, the amount of splats increased. Also, high fuel and oxygen flow rates (50 and 450 l/min respectively), the solution precursor feed rate of 40 cm³/min and spray distance of 5 cm was introduced as the optimal parameter due to higher splats observed.

Keywords YSZ-40 wt% Al₂O₃ · Solution precursor · High velocity flame spraying · Single scan experiment

1 Introduction

Solution precursor thermal spraying (SPTS) are new potentially single-step and low-cost processes that have been successfully developed for rapid synthesizing and depositing various Nano-crystalline ceramic coatings [1–3]. The SPTS deposition process includes various stages of conversion from the aqueous precursor to molten particles and solid ceramic final product [4, 5]. Compared to powders, using liquid-based feedstock offer more flexibility in creating new composite materials, maintaining the nanostructure and creating coatings with higher performance. In these processes

a stream of the liquid metallic salt solution precursors are injected directly into the high-temperature flames and/or jets generated in the torches [6, 7]. Atomizing of liquid precursor occurs while it travels through the flame and at the same time the liquid-to-solid conversion reactions and subsequent impact to the substrate result coating formation [8, 9]. Studies of solution precursor thermal spraying have mainly been conducted in plasma spraying processes (SPPS) [8]. In addition to the SPPS process, recently, a solution precursor high-velocity flame spraying (SP-HVFS) process has been successfully developed at university of Connecticut by Chen et al. [10] to deposit ceramic coatings. The results showed that microstructures of solution precursor high-velocity flame spray coatings are different from conventional HVOF process, and mainly compose of pancake-like ultrafine splats which are about ten times smaller than the splats in conventional HVOF coatings. Also it was found that the liquid

✉ Saeid Taghi-Ramezani
s.ramezany2013@gmail.com

¹ Faculty of Materials and Manufacturing Technologies,
Malek Ashtar University of Technology, Tehran, Iran

droplets experience solvent evaporation, pyrolysis, melting/semi melting and solidification processes in the HVOF flame jet. Since, both microstructure and properties of the coatings are strongly influenced by the structure of the splats [11, 12], therefore, a key step in understanding and improving thermal spray coatings is study of the formation of the coatings, through the single splats [13, 14].

The solution precursor high-velocity flame spraying is a suitable method for producing dense coatings with nanostructure. Similar to the powder HVOF process, in the liquid injection high-velocity flame spraying, the coating properties are a direct result of the high velocity of the particles in the supersonic gas stream and are useful for applications that require low porosity coatings [15, 16]. However, due to the high velocity and low temperature flame, high melting point ceramics may not be deposited [17].

Yttria-stabilized zirconia (YSZ) is the most commonly used electrolyte for high-temperature SOFC due to its high oxide ion conductivity and stability in oxidizing and reducing atmospheres [18, 19]. However, zirconia has low fracture toughness and poor strength. The addition of alumina to YSZ has been found to make it stronger, harder, lighter and stiffer at room temperature as well as at 1000 °C [18]. Among other ceramics, ZrO_2 - Al_2O_3 has a relatively high coefficient of thermal expansion, which increases its thermal shock resistance. Also, some properties of ZrO_2 - Al_2O_3 such as high fracture toughness, resistance to crack growth [20] and excellent long-term biocompatibility make it a very promising material for in vivo use with high biological safety [21]. In addition, zirconia-alumina composites have been widely used as protective coatings due to their excellent mechanical and thermal properties [10, 22]. Diffusion barrier and wear resistant coatings are among the applications of such coatings that require low porosity and high adhesion. In the ZrO_2 - Al_2O_3 binary system, there is a eutectic with composition of ZrO_2 -40 wt% Al_2O_3 at 1860 °C [23]. Because the eutectic temperature is lower than the melting points of pure zirconia (~ 2700 °C) and pure alumina (~2050 °C), the droplets with this eutectic composition will be easily melted/softened compared to the pure zirconia and alumina [6] in the HVOF flame.

The properties of composite coatings can be improved by its microstructure [24, 25]. On the other hand, The microstructure of thermal spray coating is closely related to the spray parameters [26], therefore it is important to find out the correct spray parameters such that a high fraction of the molten mass can be deposited on the substrate [27]. Also, in the solution precursor high-velocity flame spray process, the precursor is injected in the form of liquid and undergoes various thermo-physical changes before deposition. The coating microstructure can be intentionally varied over a wide range by controlling the spray parameters and relative proportions of the different stages of the precursor reaction

[5, 28]. In the present work, solution precursor that results eutectic composition of YSZ-40 wt% Al_2O_3 was high-velocity flame sprayed onto glass substrates and microstructure of the deposited material was investigated. Various processing parameters includes fuel and oxygen flow rate, solution precursor feed rate and spray distance.

2 Experimental Procedure

The solution precursors were prepared by making saturated solution of metal nitrates into deionized water. An aqueous solution containing zirconium oxy-nitrate and yttrium nitrate salts were used as YSZ precursor. The amounts of these salts in the solution were selected to result 93 wt% ZrO_2 and 7 wt% Y_2O_3 (7YSZ) after pyrolysis. Also, Aluminum nitrate salt was used as Al_2O_3 precursor. The YSZ and Alumina precursors were mixed according to the final composition of YSZ-40 wt% Al_2O_3 after pyrolysis. HVOF torch with axial liquid injection capability was used as precursor thermal spray equipment. The schematic of the SP-HVFS system is shown in Fig. 1. Compressed natural gas (CNG) and oxygen were used as the fuel gas and oxidant gas, respectively.

The different spray parameters were designed to investigate the processing characteristics of depositing YSZ-40 wt% Al_2O_3 coating by solution precursor high-velocity flame spraying. Spray distance, solution feed rate and fuel and oxygen flow rates were selected as the experimental variables. To make a clear distinction, the experiments were divided into two series of A and B. In A, oxygen with flow rate of 300 l/min and CNG with flow rate of 30 l/min and in B, oxygen with flow rate of 450 l/min and CNG with flow rate of 50 l/min were used. Also, three solution precursor flow rates of 20, 40, 60 cm^3/min at spray distances of 5 and 10 cm were used. The detailed SP-HVFS parameters are summarized in Table 1.

To study the effect of spray parameters on the microstructural features of the coatings, single scan experiments on 2.5×2.5 cm glass specimens were done. The glass specimens had a surface roughness (R_a) of 0.035 ± 0.011 μm measured by mitutoyo sj-201 surface roughness tester. Before spraying, the substrates were cleaned with acetone to remove surface contaminations. Sealed solution precursor vessel was pressurized by N_2 gas to 5 bar and so the solution precursor flows out of vessel to a liquid flow meter that controls the flow rate of solution to selected values. Solution with controlled flow rate enters axially to the high velocity jet and after atomization is propelled toward the glass specimens. In the single scan experiment, glass substrates mounted on a specimen holder of the specially designed fixture pass vertically through the flame fixed at selected distance with speed of about 1.0 m/s as shown in Fig. 2.

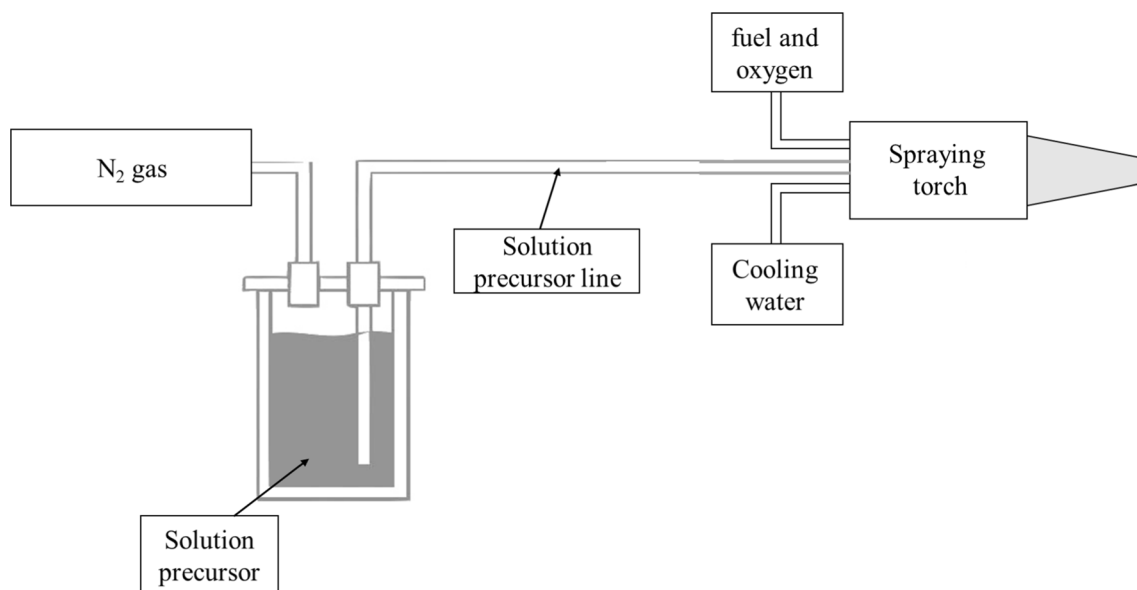


Fig. 1 Schematic illustration of the SP-HVFS Process

Table 1 Parameters of solution precursor high-velocity flame spraying used in this study

Parameter	Compressed natural gas flow rate (CNG) (l/min)	Oxygen flow rate (l/min)	Spray distance (cm)	Liquid feed rate (cm ³ /min)
A	300	30	5	20
				40
				60
			10	20
				40
				60
B	450	50	5	20
				40
				60
			10	20
				40
				60

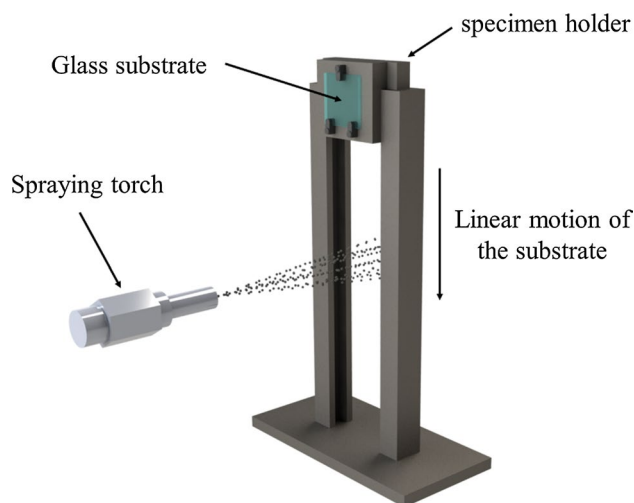


Fig. 2 Schematic illustration of the single scan experiment on a glass substrate

In this way, it is possible to examine the individual coating microstructural features such as un-pyrolysed precursor, unmelted or re-solidified particles and splats. The schematic of the single scan experiment setup on a glass substrate is shown in Fig. 2. The morphology of deposits formed on glass specimens were characterized by secondary electron (SE) mode of Field Emission Scanning Electron Microscope (SEM; VEGA\\TESCAN, Czech Republic).

Decomposition analysis were carried out by Thermo-Gravimetry (TG) combined with Differential Scanning

Calorimetry (DSC) (model STA 409 C; Netzsch, Selb, Germany) in an air environment. Prior to the TGA-DSC tests, prepared solution precursor dried on a hot plate at 50 °C for 10 h to obtain homogenous precursor powder. Thermal analysis data for dried YSZ-40 wt% Al₂O₃ precursor was recorded from room temperature up to 1100 °C at a heating rate of 10 °C/min.

3 Results and Discussion

In order to understand the transformations of the solution precursor as a result of heating, TGA-DSC analysis was performed. Figure 3 shows the weight change of the precursor by increasing temperature from room temperature up to 1100 °C. Also, the schematic illustration of transformations of precursor while it passes through the flame jet including evaporation of water, droplet break-up, gelation and precipitation, pyrolysis, sinter and melting is attached to Fig. 3. Of course, it should be noted that all atomized droplets don't undergo all of these changes necessarily. In fact this is the reason for different microstructural features present in the coating. The real aim of investigating the spray parameters in solution precursor spraying processes is to increase the portion of droplets that undergo all of the transformations mentioned above and so formation of maximum splats in the coating microstructure.

The TGA curve shows that the YSZ-Alumina precursor is hydrous and its weight decreases with increasing temperature. Almost 40% of the powder weight is lost below 150 °C. Within this initial mass loss, two distinctive regions can be seen in the curve. The first one, with a sharp and shallow endothermic appearance at 83.23 °C corresponds to the initial, quick evaporation of the water. The sharpness of the peak shows that the precursors were prepared near the maximum solubility level, and its shallowness is due to the fact that part of the aqueous solvent was evaporated at 50 °C before the TGA-DSC analysis, as mentioned in the experimental. A similar peak was reported by Sivakumar et al. [29].

Usually, the endothermic peaks between 50 and 100 °C relate to water evaporation and up to 200 °C relate to nitrate decomposition. The results of TGA-DSC show that evaporation of the solvent ends with a sharp endothermic peak at 149.73 °C, but the weight loss continues up to a temperature of about 550 °C. After the completion of the evaporation process and complete removal of the solvent,

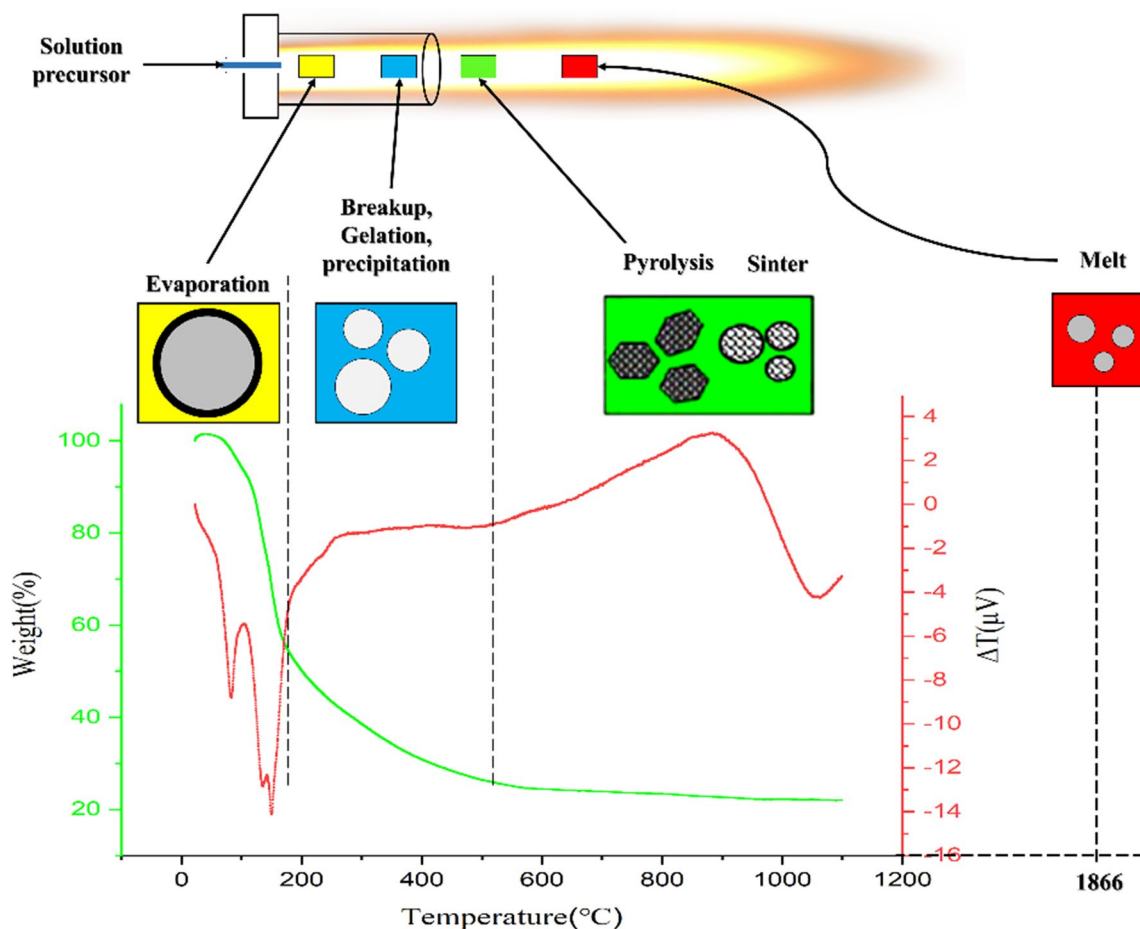


Fig. 3 TGA-DSC of the dried solution precursor, from room temperature to 1100 °C, along with a schematic illustration of Chemical and physical evolution of a droplet injected into the flame

weight loss in TG curve without observing changes in DSC can be attributed to drying of the gel-like features. From this point on (550 °C), no distinguishable weight change can be seen. In the case of the heat flow, there are two additional broad peaks, one exothermic at 874.39 °C and the other endothermic at 1063.25 °C. Since no associated weight change can be detected, the origin of such peaks could be further crystallization and phase transformation of the remaining dried material. The crystallite formation is a relative slow process with causes broadening of the exothermic peaks [9]. Hence, the only exothermic DTA peak in this graph at 874.39 °C, without remarkable weight loss attributes to the crystallization of amorphous phase. The area under the curve of such exothermic peak is a measure of heat release [29]. The last change in the graph is an endothermic peak at 1063.25 °C, which corresponds to a phase transformation or grain growth, presumably. To study in detail the pyrolysis and changes in phase constitution, XRD phase analysis was also done at the conclusion of the TG/DSC test on precursors heat treated at two temperatures of 874 and 1063 °C. It should be emphasized that the results of TGA-DSC are to gain insight on the thermodynamic behavior of the solution and only show the successive stages of the possible physical and chemical reactions [12]. Although, during the spraying process, the maximum flame temperature is higher than crystallization and melting temperature of the coating material, but as mentioned before, for all injected droplets, all steps shown in Fig. 3 will not be completed, due to kinetics of the reactions. This indicates that depending on the temperature history of the droplets in the flame, they undergo different changes and contribute in coating microstructures as different aspects such as splats, un-pyrolysed precursor and un-melted or re-solidified particles.

The XRD patterns of heat treated precursor at two critical temperatures of 874 °C and 1063 °C determined by thermal analysis test are shown in Fig. 4. X-ray diffraction patterns in Fig. 4 show that in both heat treating temperatures, the main peaks are related to tetragonal ZrO_2 . This shows that YSZ is the base composition of the composite. The presence of Al_2O_3 in the XRD results wasn't proved probably because Al_2O_3 precursor wasn't pyrolysed completely and or the amount of pyrolysed Al_2O_3 precursor wasn't enough to show itself in XRD results. Also, it can be concluded that, the heat-treated precursor at 874 °C hasn't a fully-crystalline structure and with the increase of the heat-treatment temperature to 1063 °C, no phase transition occurs and only the relative intensity of the diffraction peaks increases, which indicates increasing the degree of crystallinity. In addition, another parameter that changes the intensity or peak broadening in X-ray diffraction analysis is grain size [30]. It seems that with the increase in the heat treatment temperature, the average grain size of the nanopowder has also increased. This change can be related to the endothermic peak in TGA analysis. In the following, the results of the single scan experiment are given.

Twelve different spray runs (two fuel and oxygen flow rates, three solution precursor feed rates and two spray distances), as described in the experimental methods section, were performed. Figure 5 shows images of deposits formed in single scan experiments on glass specimens at solution precursor feed rate of 20 cm³/min, spray distance of 5 cm and flame parameter A (Table 1). The high-magnification image confirms that the microstructure is uniform with no presence of un-pyrolysed precursor and mainly compose of splats with thickness of less than 100 nm which are about ten times smaller than the splats in conventional HVOF coatings. In the SP-HVOF process, when molten/semi-molten

Fig. 4 XRD patterns of heat treated precursor

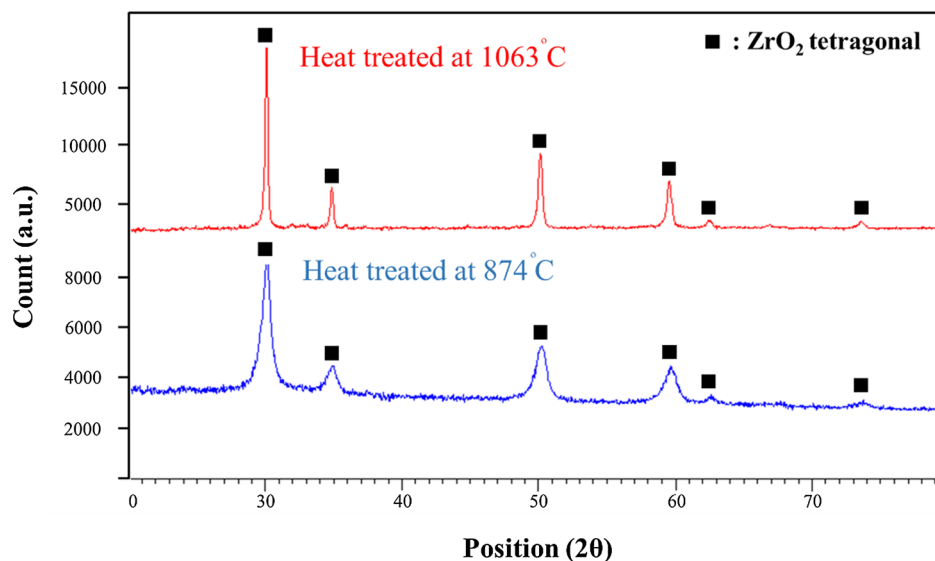
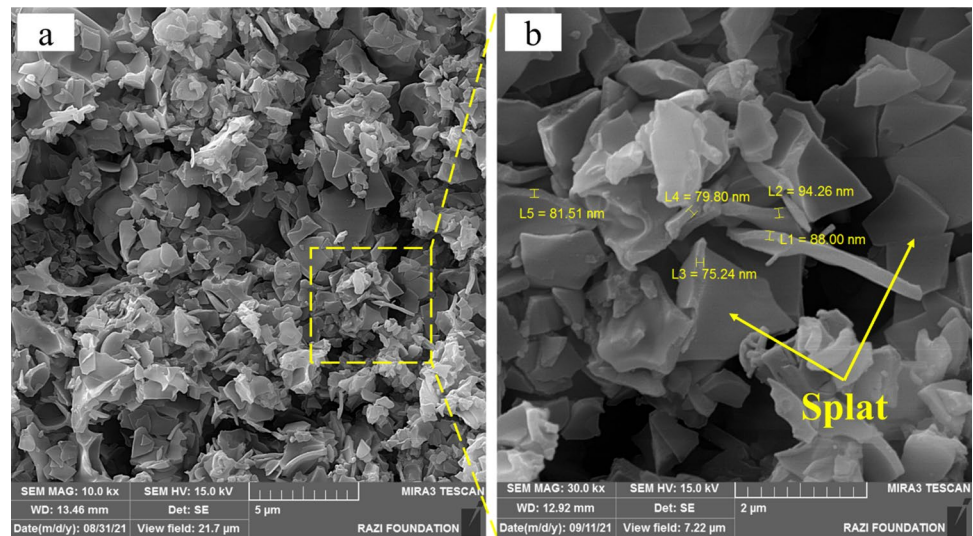


Fig. 5 FE-SEM images of deposit formed in single scan experiments on glass specimens at solution precursor feed rate of $20 \text{ cm}^3/\text{min}$, spray distance of 5 cm and flame parameter A



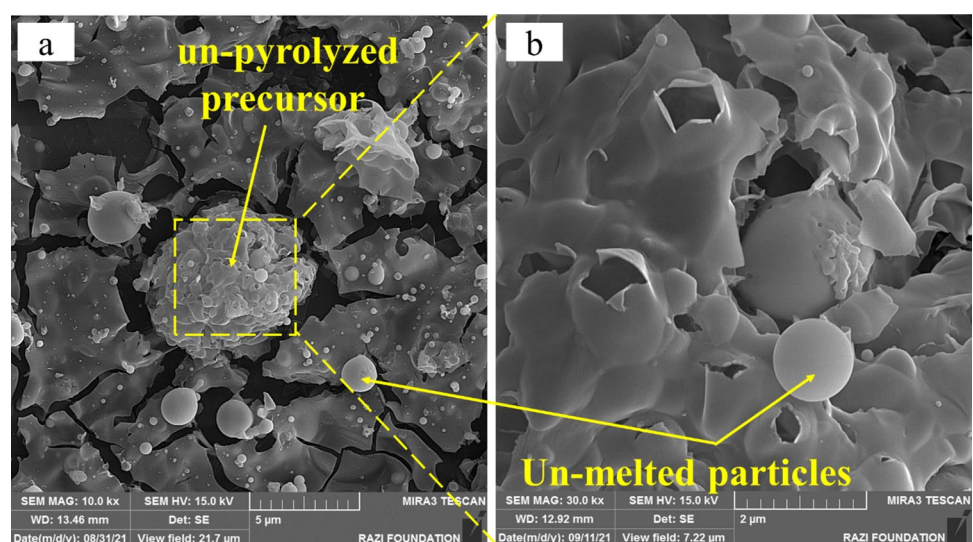
particles impact to the substrate with high velocity, they will spread and form the splats [10]. The formation of fine splats is characteristic of the high-velocity flame spraying process and coating formation from the liquid phase [31, 32]. Also, these splats clearly indicate that the liquid droplets have experienced all of the solvent evaporation, pyrolysis, melting/semi melting processes in the HVOF flame jet.

Figure 6 shows images of deposits formed in single scan experiments on glass specimens at solution precursor feed rate of $40 \text{ cm}^3/\text{min}$ and spray distance of 5 cm and flame parameter A. The microstructural features of deposit formed at solution precursor feed rate of $40 \text{ cm}^3/\text{min}$ (Fig. 6) are totally different from the deposit formed at solution precursor feed rate of $20 \text{ cm}^3/\text{min}$ (Fig. 5). In Fig. 6 it can be seen that the deposit consists mainly of a fractured, mud-like film with loosely bonded solid spheres ($\sim 1 \mu\text{m}$). It seems that in this case the conditions of solution atomization are

such that the droplets in the flame jet undergo incomplete solvent evaporation and form mud-like film upon impact the substrate.

The high magnification image (Fig. 6b) shows gel-like structures along with hollow shells. Models based on aerodynamic droplet break-up, evaporation of droplets and solute precipitation have been developed for the formation of fractured hollow shell structures [10]. It seems that hollow shells are formed in large droplets. Virendra [27] confirms that small droplets tend to precipitate volumetrically to form solid particles while in large droplets, the solvents are first removed by exposure to high temperatures, leading to increase in solution concentration up to saturation [29]. Furthermore, previously published droplet modeling studies focusing on SPPS confirm that the diffusive transport within the droplet is much slower than the rapid increase in solute concentration through evaporation, leading to the

Fig. 6 FE-SEM images of deposit formed in single scan experiments on glass specimens at solution precursor feed rate of $40 \text{ cm}^3/\text{min}$, spray distance of 5 cm and flame parameter A



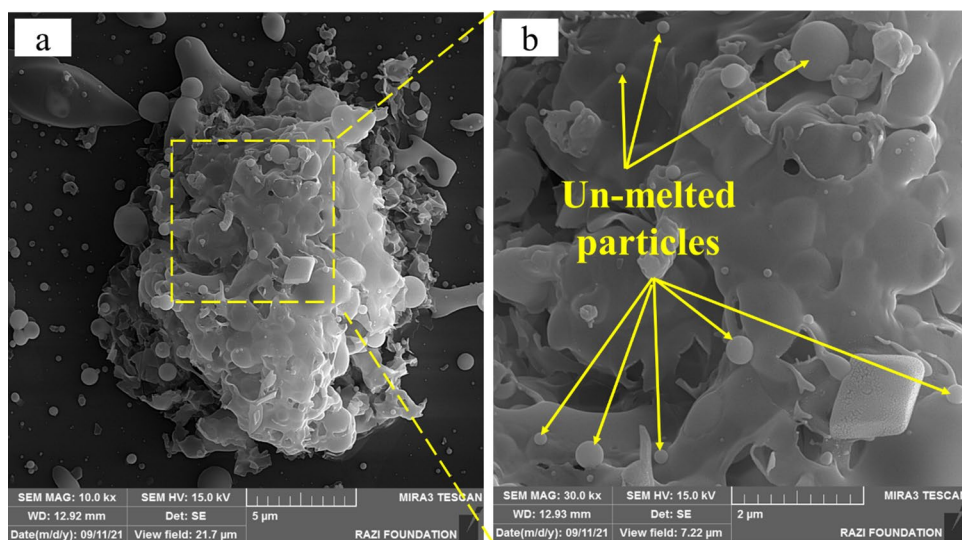
formation of a highly concentrated solution near the surface [33]. Therefore, when the saturation concentration is reached, solute precipitation begins near the droplet surface and likely forms an impermeable thin layer shell that encapsulates the liquid. This thin shell with high concentration of solutes can prevent further evaporation, consequently, the internal pressure caused by the buildup of vapor inside the droplet leads to swell and burst. The hollow-shell structures were also observed by Valefi [34] and Chen [35]. The simulation results conducted by Jordan et al. [5], admit the possibility that hollow droplets may form and also vapor explosion from internal evaporation is one possible mechanism for droplet break-up.

Figure 7 shows images of deposit formed in single scan experiments on glass specimens at solution precursor feed rate of $60 \text{ cm}^3/\text{min}$, spray distance of 5 cm and flame parameter A. In Fig. 7, the deposit includes un-pyrolysed precursor. The thermal history (time–temperature) of droplets injected to the flame determines the microstructural features of deposit. Depending on this history, a droplet to form the solid material on the sample surface undergoes some or all of the following processes: precursor solvent evaporation, droplet breakup, precursor solute precipitation, pyrolysis, sintering, melting and crystallization [36]. Deposit forms on the sample surface after undergoing some or all of these processes shown already in Fig. 3. Also, in the solution precursor thermal spraying process, evaporation of solute and pyrolysis of precursor can be done in two steps; the first step occurs when the solution precursor is injected into the flame. When the precursor droplet is exposed to the thermal flame the temperature is increased at the surface. As a result, the solvent evaporate and the precursor undergo a thermal decomposition process similar to that shown in Fig. 3, forming a solid, and then pyrolysis, crystallization and melting can occur [22]. In this stage, evaporation of precursor solute

or pyrolysis reactions may not be done completely. At the second step depending on preheating temperature of substrate and the heat transferred from torch to substrate solute evaporation or pyrolysis reactions can occur on the substrate. It is obvious that in single scan experiments because of high speed traverse of glass specimens relative to the torch, little heat transfers to the specimens and the reactions that happen on the substrate are removed. In such conditions, physical and chemical reactions perform only in the first stage. From the above discussion it can be concluded that precursor reach the substrate surface in different conditions.

With Careful study at high-magnification (Fig. 7b), it can be seen that the spherical particles with different sizes present in addition to irregular gel-like features. This spherical particles are atomized particles that do not get enough heat for pyrolysis and crystallization. In fact, in the solution precursor thermal spraying processes, the liquid can be injected to jet/flame and atomized by the high velocity flame or can be atomized prior to injection [37]. Because in this study, there isn't any atomizer, therefore due to shear stress caused by the flowing gas, the solution precursor undergoes atomization as injects in to the flame jet [12] which form finely sized droplets. In such a situation, only spray parameters determine the atomizing conditions of the injected precursor. It seems that the different sizes of un-melted particles are related to the atomization condition in these spray parameters. Also, the injection rate of the solution precursor in Fig. 7 was 1.5 and 3 times greater than the parameter used in Figs. 5 and 6, respectively. Therefore, it is logical to presume that the use of a higher solution precursor feed rate limits the heat transferred to the precursor droplets and leads to greater retention of gel-like features and un-melted particles. Tania et al. [38] have shown that the precursor droplets tend to form a gel during evaporation, which is responsible for the type of aggregate morphology observed in Fig. 6.

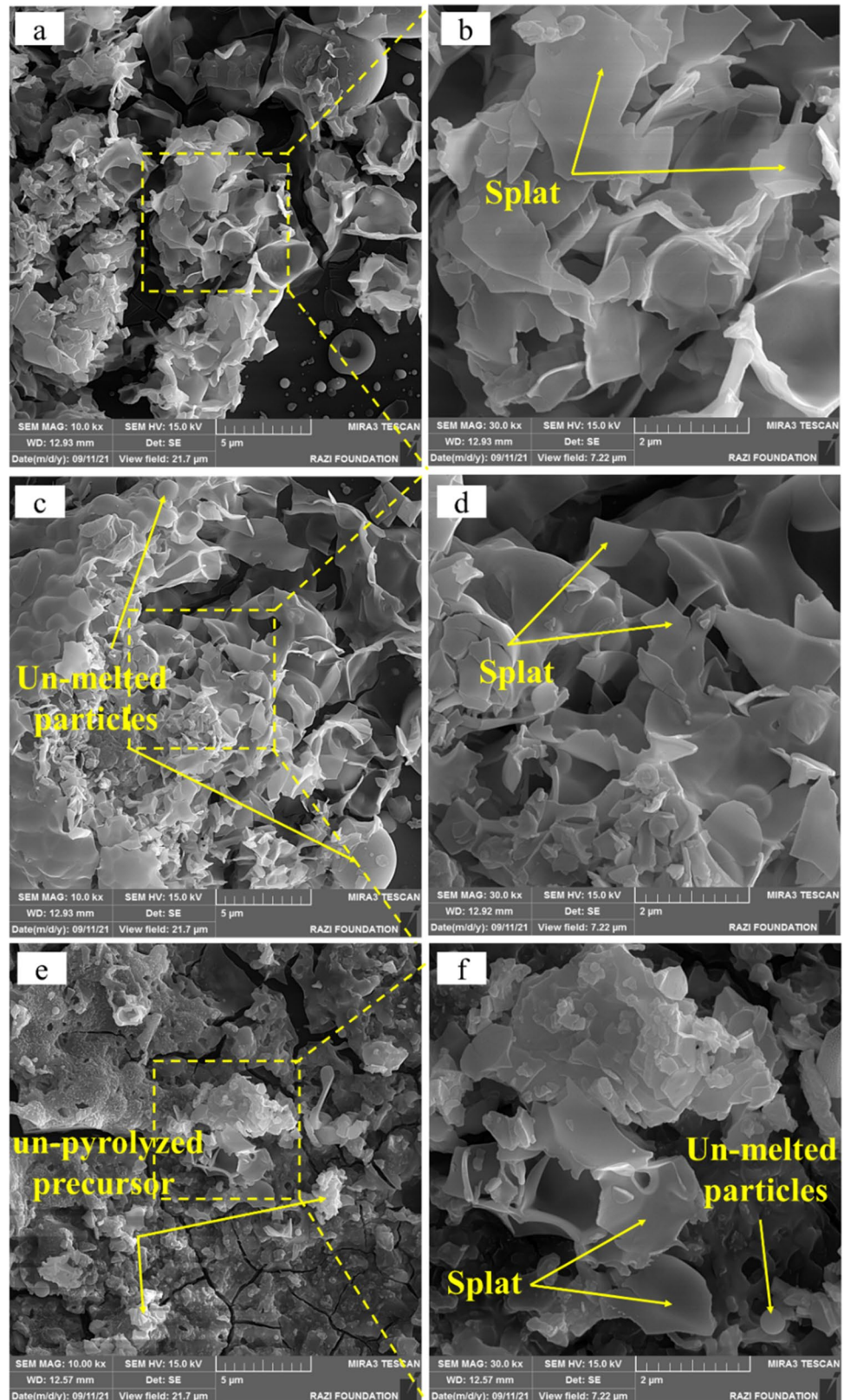
Fig. 7 FE-SEM images of deposit formed in single scan experiments on glass specimens at solution precursor feed rate of $60 \text{ cm}^3/\text{min}$, spray distance of 5 cm and flame parameter A



The Morphologies of deposits formed under different solution precursors at spray distance of 10 cm and flame

parameter A are shown in Fig. 8. Samples a to f have identical spray parameters except for the solution precursor feed

Fig. 8 FE-SEM images of deposits formed in single scan experiments on glass specimens at solution precursor feed rates of **a** 20, **c** 40 and **e** 60 cm³/min at spray distance of 10 cm and flame parameter A



rate. As noted in the Fig. 3, precursor in various stages of heating reaches the surface and contributes different features in the microstructure. It can be seen that non-decomposed precursor were not found on deposits formed at 20 and 40 cm^3/min solution precursor feed rates, while at the solution feed rate of 60 cm^3/min , besides splats and un-melted particles, non-decomposed precursor can be observed. This can be due to the using higher solution precursor feed rate. Increasing the solution precursor feed rate, transfers less heat to injected precursor and so it can be expected that a fewer number of droplets will undergo the final processes by which melting occurs [39]. Also, the effect of solution precursor feed rate on atomization condition should be considered. It seems that increase in the solution precursor feed rate results in weaker atomizing of solution precursor. In addition, at 60 cm^3/min solution precursor feed rates, some mud-like cracks are also seen in the deposit. This clearly shows that, during the SP-HVFS process, some precursor reaches the substrate as un-pyrolysed. Based on thermal analysis, Fauchais et al. [40] confirmed that the un-pyrolysed precursor contains significant amounts of water. The mud-like cracks are the result of shrinkage due to aqueous solvent evaporation, presumably. This cracks also observed by saremi [39] and Chen [4].

Figure 9a to f shows images of deposits formed in single scan experiments on glass specimens at solution precursor feed rates of 20, 40 and 60 cm^3/min at spray distance of 5 cm and flame parameter B. Three general features of the deposit morphology are realized depending on the spray parameters which are; precursor droplets that reached and spread on the glass surface, non-decomposed precursor and spheres. Microstructural changes under different parameters could be seen more clearly in high magnification images. Unexpectedly, it can be seen that layers formed at solution precursor injection rate of 20 cm^3/min contains non-decomposed precursor. As previously noted, in the SP-HVFS process, the solution precursor is fed axially in to the torch and liquid–jet interaction causes fragmentation of the liquid into fine droplets [41]. In this parameter, the flow rate of fuel and oxygen increased, and the shock diamonds were also clearly seen at the flame jet. It seems that at the solution feed rate of 20 cm^3/min , the condition of the liquid atomization by shock diamonds causes non-uniform distribution of the particles in the flame.

The microstructure of deposits formed at solution precursor injection rate of 40 cm^3/min spray distance of 10 cm and flame parameter B (Fig. 9c, d) is similar to that of solution precursor feed rate of 20 cm^3/min , spray distance of 5 cm and flame parameter A (Fig. 5). As can be seen, they are mainly composed of ultrafine splats and the cracked mud-like film and semi-pyrolysed hollow shell structures have disappeared. This microstructure confirm improved degree of melting and splat formation that can be due to the higher flame enthalpy that resulted from using parameter

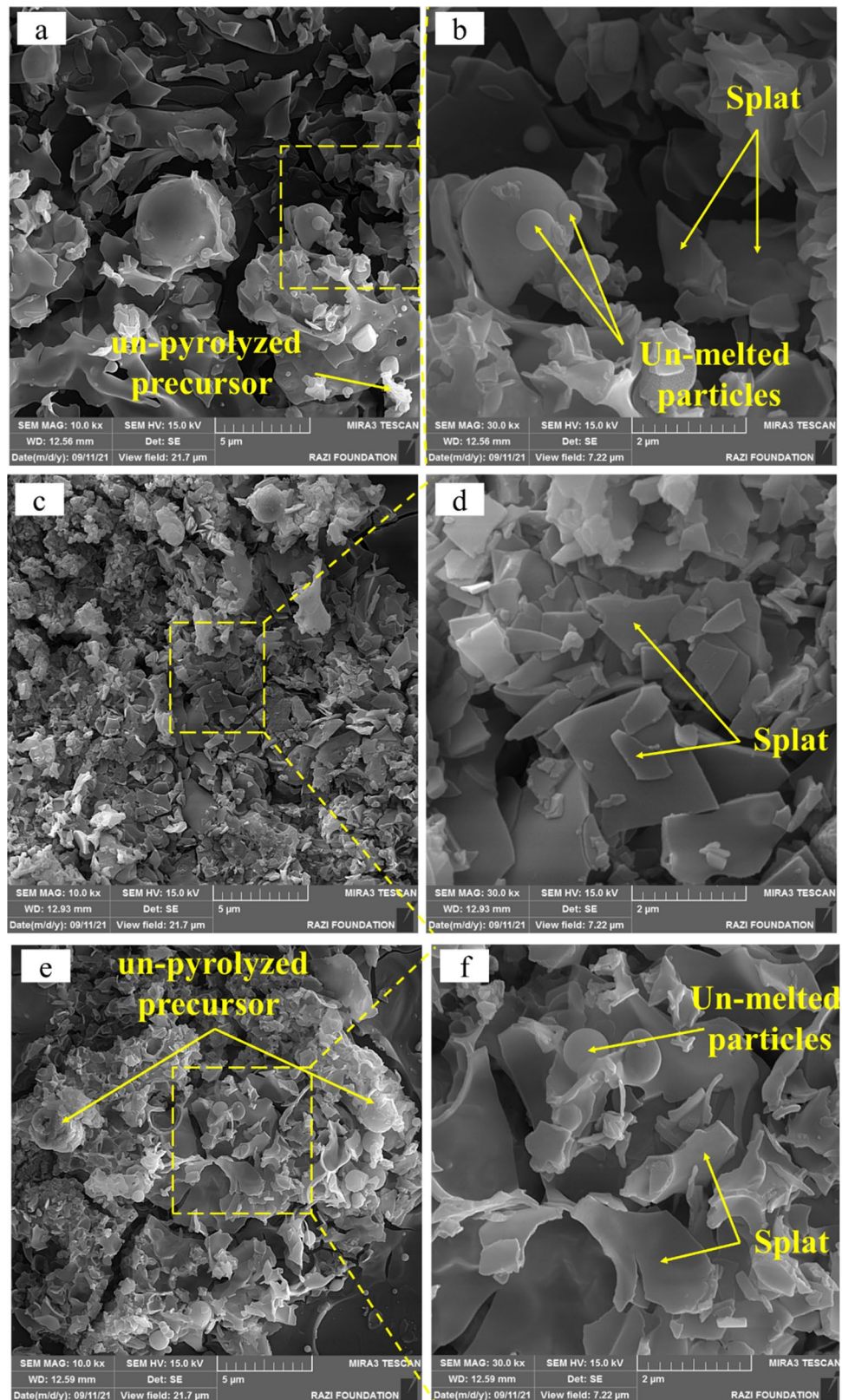
B. Increase in thermal energy promotes pyrolysis of the precursor and subsequent melting of particles formed. Also, similar to other liquid feedstock thermal spraying, in SP-HVFS Process, splat sizes are dependent on the atomization condition. Therefore, proper atomization condition affect the thermal history of injected droplets, so that as the particles become smaller, the kinetics of deposition change and the microstructure of the coating is improved [27]. Actually, in suitable atomization condition, easy droplet breakup and solvent evaporation leads to full pyrolysis and melting; while large droplet and difficult evaporation leads to incomplete evaporation [35] and the formation of un-pyrolysed or un-melted particles. The above results suggest that the atomization characteristics changes with injection rate of solution precursor and also the flame parameters that should be considered together. The suitable atomization conditions for the parameter B are obtained with the solution feed rate of 40 cm^3/min . Also, it seems that the thickness of the splats has decreased compared to Fig. 5. In fact, using higher flow rate of fuel and oxygen, in addition to increasing the enthalpy, leads to the acceleration of the flame jet and particles, which reduces the thickness of the splats.

By increasing the feed rate of the solution up to 60 cm^3/min , un-pyrolysed precursors can also be observed (Fig. 9e, f). The presence of these un-pyrolysed precursors can be attributed to an increase in the amount of solution precursor and insufficient heat per droplet and also weaker atomization.

Figure 10a to f shows images of deposits formed in single scan experiments on glass specimens at solution precursor injection rate of 20, 40 and 60 cm^3/min , spray distance of 10 cm and flame parameter B. The glass surface at solution injection rate of 40 cm^3/min (Fig. 10c, d) shows a higher degree of splats, with some solid spherical particles. This morphology of layers attribute to the higher flame enthalpy that resulted from using parameter B. Also, again it should be emphasized that the role of the atomization characteristics in controlling splat and solid particle formation and final coating microstructure can be critical, so that better atomizing conditions provide more uniform and finer particle size distribution and so the particles undergo almost similar changes during their flight in the flame. This is the trend observed in Figs. 9 and 10 for solution feed rate of 40 cm^3/min .

Figure 10c shows the microstructure of the deposit formed under the same conditions as Fig. 9c but using spray distance of 10 cm. In the spray distance of 10 cm, since the precursor dwell time in flame is longer, it is expected that the heat transferred is higher and more material has been molten. But, a very small fraction of un-melted spherical particles were observed when spray distance was doubled, which could be attributed to the re-solidifying of the particles at longer spray distances. The calculated results by Cheng et al.

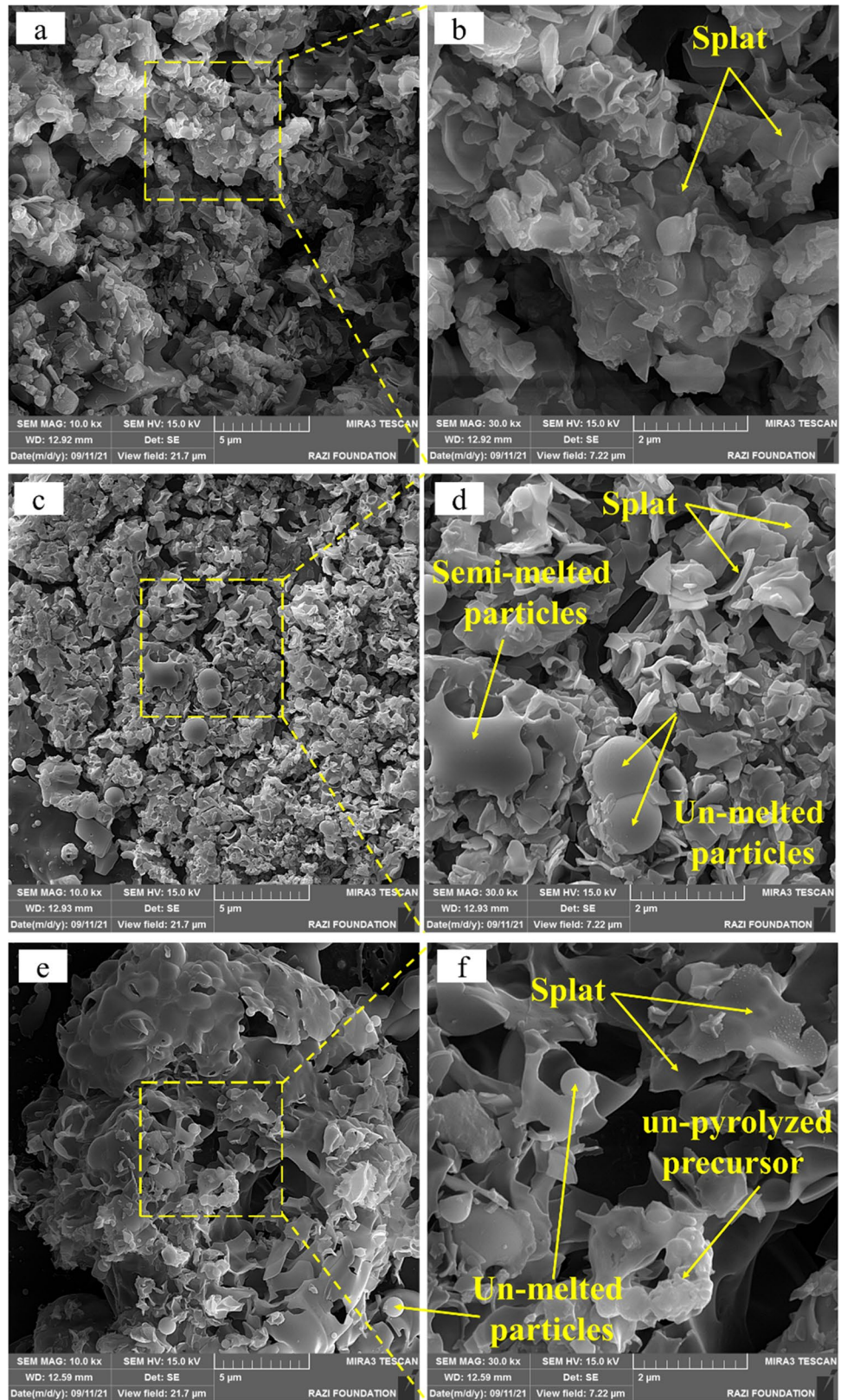
Fig. 9 FE-SEM images of deposits formed in single scan experiments on glass specimens at solution precursor feed rates of **a** 20, **c** 40 and **e** 60 cm³/min, spray distance of 5 cm and flame parameter B



[42] showed that the physical status of particles before hitting onto the substrate which is determined by the velocity and temperature of the particles, is a key factor affecting

the microstructure of the coatings and is strongly influenced by the particle size, morphology and spray distance. In fact, in thermal spraying processes, the velocities and

Fig. 10 FE-SEM images of deposits formed in single scan experiments on glass specimens at solution precursor feed rates of **a** 20, **c** 40 and **e** 60 cm³/min, spray distance of 10 cm and flame parameter B



temperatures of small particles decrease more severely than larger particles due to their smaller momentum and thermal inertias, while larger particles will reach the maximum temperature and velocities in a longer spray distance [43]. In the SP-HVFS process, after evaporation, decomposition and pyrolysis of the droplets, the mass of the particles become small, resulting in reduced momentum. Therefore, small particles may reach the melting point in a short time, but at longer spray distance due to the lower temperature of the flame jet at farther distances [28], molten particles may re-solidify during the flight. Similar to what happened in parameter A, the melting state of the coating became worse with increasing solution flow rate up to 60 cm³/min and un-pyrolysed precursors also increased.

4 Conclusion

The aim of this study was to investigate the influence of the Solution precursor high velocity flame spraying parameters, such as fuel and oxygen flow rates, spray distance and solution precursor feed rate on splat formation of the YSZ-40 wt% Al₂O₃ by single scan experiment. The results indicated that the microstructures of the deposited layers were sensitive to the spray parameters considerably. Some important results can be summarized as follows:

1. The results of the thermal decomposition, first reflected the successive evaporation of water and nitrates, and it was manifested in the form of continuous loss in weight. Also the XRD results on heat treated precursor showed that no phase transition occurred with the increase of heat treatment temperature from 874 to 1063 °C and the increase in peak intensity is the result of the increase in the crystallinity degree and grain growth.
2. The formation of hollow particles is the result of the high surface evaporation rates that leads to increased solute concentration near the surface and the formation of a solid shell with some amount of retained precursor within. The internal pressure caused by the buildup of vapor inside the droplet will lead to inflate and rupture.
3. By increasing the solution precursor feed rate up to 60 cm³/min, the amount of un-pyrolysed precursor and unmelted particles in the microstructure increased.
4. Atomization characteristics that is determined by flame parameters and precursor feed rate, are important in determining flame stability, formation of un-pyrolysed precursor, spherical solid particle, controlling splat formation and final coating microstructure.
5. Spray distance is an important factor which affect the microstructure. Due to smaller sizes of the particles in SP-HVFS process, the shorter spray distance (5 cm) allows more particles deposition in molten condition on substrate. For longer spray distance, particles may solidify during the flight.
6. Despite the fact that the precursor droplets at longer spray distances have a greater chance of undergoing pyrolysis and crystallization reactions, but the results showed that the droplets are exposed to heat up to a certain distance in the flame and their temperature decrease with increasing distance. This can be a reason for re-solidifying of some particles before reaching the substrate.
7. According to the obtained results, it seems that the deposition condition using the high velocity flame spray parameter A, at the solution feed rate of 20 cm³/min and the spraying distance of 5 cm and also, spray parameter B, at the solution feed rate of 40 cm³/min and the spraying distance of 5 cm is suitable.

Declarations

Conflict of interest The authors declare that they have no known competing financial interests or personal relationships that could have appeared to influence the work reported in this paper.

References

1. M. Gell, L. Xie, X. Ma, E.H. Jordan, N.P. Padture, Highly durable thermal barrier coatings made by the solution precursor plasma spray process. *Surf. Coat. Technol.* **177**, 97–102 (2004)
2. A. Jadhav, N.P. Padture, F. Wu, E.H. Jordan, M. Gell, Thick ceramic thermal barrier coatings with high durability deposited using solution-precursor plasma spray. *Mater. Sci. Eng. A* **405**(1–2), 313–320 (2005)
3. L. Xie, X. Ma, E.H. Jordan, N.P. Padture, D.T. Xiao, M. Gell, Deposition mechanisms of thermal barrier coatings in the solution precursor plasma spray process. *Surf. Coat. Technol.* **177**, 103–107 (2004)
4. C. Jiang, D. Cietek, R. Kumar, E.H. Jordan, Ytterbium silicate environmental barrier coatings deposited using the solution-based precursor plasma spray. *J. Therm. Spray Technol.* **29**(5), 979–994 (2020)
5. E.H. Jordan et al., Superior thermal barrier coatings using solution precursor plasma spray. *J. Therm. Spray Technol.* **13**(1), 57–65 (2004)
6. D. Chen, E.H. Jordan, M. Gell, X. Ma, Dense alumina–zirconia coatings using the solution precursor plasma spray process. *J. Am. Ceram. Soc.* **91**(2), 359–365 (2008)
7. A. Ganvir, Microstructure and thermal conductivity of liquid feed-stock plasma sprayed thermal barrier coatings, University West, 2016.
8. J. Puranen, J. Laakso, M. Kylmälahti, P. Vuoristo, Characterization of high-velocity solution precursor flame-sprayed manganese cobalt oxide spinel coatings for metallic SOFC interconnectors. *J. Therm. Spray Technol.* **22**(5), 622–630 (2013)
9. J. Puranen et al., High temperature oxidation tests for the high velocity solution precursor flame sprayed manganese–cobalt oxide spinel protective coatings on SOFC interconnector steel. *Int. J. Hydrog. Energy* **40**(18), 6216–6227 (2015)

10. D. Chen, E.H. Jordan, M. Gell, Solution precursor high-velocity oxy-fuel spray ceramic coatings. *J. Eur. Ceram. Soc.* **29**(16), 3349–3353 (2009)
11. M. Alotaibi, Application of an image-based model of the elastic modulus of porous thermal barrier coatings. *Met. Mater. Int.* **28**(8), 1794–1808 (2022)
12. D. Tejero-Martin, Z. Pala, S. Rushworth, T. Hussain, Splat formation and microstructure of solution precursor thermal sprayed Nb-doped titanium oxide coatings. *Ceram. Int.* **46**(4), 5098–5108 (2020)
13. J. Mostaghimi, S. Chandra, Splat formation in plasma-spray coating process. *Pure Appl. Chem.* **74**(3), 441–445 (2002)
14. S. Brossard, *Microstructural Analysis of Thermal Spray Coatings by electron Microscopy*, University of New South Wales, Sydney 2010.
15. X. Chen, C. Li, S. Li, X. Han, H. Jiang, X. Zhao, HVOF spray performance optimization analysis and experimental research of WC–12Co coating on Ti alloy. *Met. Mater. Int.* (2023). <https://doi.org/10.1007/s12540-023-01458-y>
16. G. Bolelli, J. Rauch, V. Cannillo, A. Killinger, L. Lusvardi, R. Gadow, Microstructural and tribological investigation of high-velocity suspension flame sprayed (HVSFS) Al₂O₃ coatings. *J. Therm. Spray Technol.* **18**, 35–49 (2009)
17. T. Sidhu, S. Prakash, R. Agrawal, Studies on the properties of high-velocity oxy-fuel thermal spray coatings for higher temperature applications. *Mater. Sci.* **41**, 805–823 (2005)
18. S. Choi, N. Bansal, Mechanical behavior of zirconia/alumina composites. *Ceram. Int.* **31**(1), 39–46 (2005)
19. N.P. Bansal, D. Zhu, Thermal conductivity of zirconia–alumina composites. *Ceram. Int.* **31**(7), 911–916 (2005)
20. D. Casellas, I. Ràfols, L. Llanes, M. Anglada, Fracture toughness of zirconia–alumina composites. *Int. J. Refract. Met. Hard Mater.* **17**(1–3), 11–20 (1999)
21. P. Fabbri, C. Piconi, E. Buresi, G. Magnani, F. Mazzanti, C. Mingazzini, Lifetime estimation of a zirconia–alumina composite for biomedical applications. *Dent. Mater.* **30**(2), 138–142 (2014)
22. S. Taghi-Ramezani, Z. Valefi, M. Mirjani, R. Ghasemi, The influence of pyrolysing Al₂O₃ precursor on the high temperature properties of the YSZ–Al₂O₃ composite coating. *Surf. Eng.* **37**(8), 991–1001 (2021)
23. M. Saremi, Z. Valefi, N. Abaeian, Hot corrosion, high temperature oxidation and thermal shock behavior of nanoagglomerated YSZ–alumina composite coatings produced by plasma spray method. *Surf. Coat. Technol.* **221**, 133–141 (2013)
24. J.G. Thakare, C. Pandey, M. Mahapatra, R.S. Mulik, Thermal barrier coatings: a state of the art review. *Met. Mater. Int.* **27**(7), 1947–1968 (2021)
25. Y. Wang, C. He, B. Hockey, P. Lacey, S. Hsu, Wear transitions in monolithic alumina and zirconia–alumina composites. *Wear* **181**, 156–164 (1995)
26. H. Kwon et al., Effect of process-gas composition on in-flight and deposition characteristics of atmospheric plasma-sprayed Ni particles. *Met. Mater. Int.* **29**(6), 1825–1840 (2023)
27. V. Singh, R. Draper, S. Seal, Effect of processing parameters on cerium oxide coating deposition in solution precursor plasma spray. *J. Am. Ceram. Soc.* **96**(8), 2437–2444 (2013)
28. T. Yang, W. Ma, X. Meng, W. Huang, Y. Bai, H. Dong, Deposition characteristics of CeO₂–Gd₂O₃ co-stabilized zirconia (CGZ) coating prepared by solution precursor plasma spray. *Surf. Coat. Technol.* **381**, 125114 (2020)
29. S. Govindarajan, R.O. Dusane, S.V. Joshi, In situ particle generation and splat formation during solution precursor plasma spraying of yttria-stabilized zirconia coatings. *J. Am. Ceram. Soc.* **94**(12), 4191–4199 (2011)
30. Y. Zhao et al., Effects of calcination temperature on grain growth and phase transformation of nano-zirconia with different crystal forms prepared by hydrothermal method. *J. Mater. Res. Technol.* **19**, 4003–4017 (2022)
31. M. Oksa, E. Turunen, T. Suhonen, T. Varis, S.-P. Hannula, Optimization and characterization of high velocity oxy-fuel sprayed coatings: techniques, materials, and applications. *Coatings* **1**(1), 17–52 (2011)
32. H. Hu, L. Mao, S. Yin, H. Liao, C. Zhang, Wear-resistant ceramic coatings deposited by liquid thermal spraying. *Ceram. Int.* **48**, 33245–33255 (2022)
33. D. Chen, E.H. Jordan, M. Gell, Effect of solution concentration on splat formation and coating microstructure using the solution precursor plasma spray process. *Surf. Coat. Technol.* **202**(10), 2132–2138 (2008)
34. Z. Valefi, M. Saremi, The effects of plasma spray parameters on the microstructure and phase composition of thermal barrier coatings made by SPPS process. *Iran. J. Mater. Sci. Eng.* **14**(2), 11–23 (2017)
35. D. Chen, E.H. Jordan, M. Gell, The solution precursor plasma spray coatings: influence of solvent type. *Plasma Chem. Plasma Process.* **30**(1), 111–119 (2010)
36. W. Fan, Y. Bai, Review of suspension and solution precursor plasma sprayed thermal barrier coatings. *Ceram. Int.* **42**(13), 14299–14312 (2016)
37. L. Pawlowski, Suspension and solution thermal spray coatings. *Surf. Coat. Technol.* **203**(19), 2807–2829 (2009)
38. T. Bhatia et al., Mechanisms of ceramic coating deposition in solution-precursor plasma spray. *J. Mater. Res.* **17**(9), 2363–2372 (2002)
39. M. Saremi, Z. Valefi, The effects of spray parameters on the microstructure and thermal stability of thermal barrier coatings formed by solution precursor flame spray (spfs). *Surf. Coat. Technol.* **220**, 44–51 (2013)
40. P. Fauchais, A. Vardelle, Solution and suspension plasma spraying of nanostructure coatings, in *Advanced Plasma Spray Applications*, ed. by H.S. Jazi (IntechOpen, London, 2012), pp. 149–188
41. W. Yang, M. Jia, K. Sun, T. Wang, Influence of density ratio on the secondary atomization of liquid droplets under highly unstable conditions. *Fuel* **174**, 25–35 (2016)
42. D. Cheng, Q. Xu, E. Lavernia, G. Trapaga, The effect of particle size and morphology on the in-flight behavior of particles during high-velocity oxyfuel thermal spraying. *Metall. Mater. Trans. B* **32**, 525–535 (2001)
43. M. Li, P.D. Christofides, Modeling and control of high-velocity oxygen-fuel (HVOF) thermal spray: a tutorial review. *J. Therm. Spray Technol.* **18**, 753–768 (2009)

Publisher's Note Springer Nature remains neutral with regard to jurisdictional claims in published maps and institutional affiliations.

Springer Nature or its licensor (e.g. a society or other partner) holds exclusive rights to this article under a publishing agreement with the author(s) or other rightsholder(s); author self-archiving of the accepted manuscript version of this article is solely governed by the terms of such publishing agreement and applicable law.